ISSN 1027-4510, Journal of Surface Investigation: X-ray, Synchrotron and Neutron Techniques, 2022, Vol. 16, No. 6, pp. 1033–1040. © Pleiades Publishing, Ltd., 2022.

Distance and Temperature Effects for the System of Chemisorbed Quantum Dot/Graphene

Fatima T. Hussein[a], * and Haider K. Fadel[a], **

[a] *Department of Physics, College of Education for Pure Sciences, University of Basrah, Basra, Iraq*

**e-mail: pgs2141@uobasrah.edu.iq*

***e-mail: haider.qassim@uobasrah.edu.iq*

Received March 15, 2022; revised May 25, 2022; accepted May 25, 2022

Abstract—Throughout the Newns–Anderson model, the chemisorption process for atom-like semiconductor spherical quantum dots on pristine pure graphene was investigated. The physical solutions for occupation of the energy levels of quantum dots are magnetic for all normal distance values away the graphene sheet, but nonmagnetic near the graphene sheet, according to self-consistent solutions. The consequences of all associated parameters are also considered.

Keywords: Anderson impurity, quantum dot, graphene, chemisorption

DOI: 10.1134/S1027451022060076

INTRODUCTION

Device miniaturization has been a major priority in both basic and applied research in recent decades. Understanding the tiniest magnetic units, consisting of several atoms or a single atom, is a critical first step in this approach. Magnetic nanostructures on insulators [1], semiconductors [2] and metals [3, 4] have been extensively studied; the discovery of graphene gave the opportunity to investigate a new substrate with intriguing electrical properties [5–7]. Monolayer graphene exhibits linear energy dispersion with massless Dirac fermions, which opens up new possibilities for spintronic devices. Only a few studies have been published [8–10], and the magnetic characteristics of a single magnetic adsorbent on graphene have yet to be explored experimentally.

The relationship between the atomic structure, electronic, and magnetic states is one of the most important aspects of the physics of nanostructures. Interatomic interactions were determined using a variety of empirical and semi-empirical potentials [11]. These reduced mathematical equations for representing interatomic forces resulting from quantum mechanical interactions are known as analytic functions of potential energy.

Graphene is a honeycomb-structure of carbon atoms that forms a 2D conductive nanomaterial [12, 13]. Its structural and chemical stability, as well as its unparalleled optical and electrical properties, make it beneficial for a variety of applications [14–18].

The ability of a substance to accept a negative charge determines the direction of electron transmission. Since the discovery [19, 20], the transport properties of graphene have been the focus of active research [21–24]. When the chemical potential is tuned in close proximity to the Dirac point, the most amazing results are obtained. When potential impurities are added to ballistic graphene at the Dirac point, it conducts better [25–27]. The most plausible reasons limiting electron mobility are "strong" impurities that cause resonances near the Dirac point ("midgap states"), which can be used for graphene functionalization. Some scatterers give as possible realizations the concentration dependence of conductivity [28] with vacancies, adsorbed atoms, molecules, or impurity clusters [29, 30]. Hydrogen atoms, which can be added to a graphene sample in a controlled manner, are an excellent example [31, 32].

At sufficiently high impurity concentrations, the interplay of the symmetries prevents quantum localization at the Dirac point [33] and generates a quantum critical regime of charge transfer. In this regime, graphene conductivity is expected to be constant, depending on the distribution of adatoms among distinct sublattices of the graphene crystal [34].

Quantum dots are tiny particles of matter containing several dozen of electrons. They are often electrically characterized in a two-dimensional electron gas at the GaAs–GaAlAs heterostructure interface. It is important to remember about quantum dots that they can be considered as solid impurities [35].

The binding of quantum dots to a graphene is known as chemisorption and refers to chemically strong bindings, as opposed to physical sorption, which refers to a weaker bond that can only be sustained on graphene at low temperatures. Chemisorption requires large amounts of energy on a chemical scale, and chemical processes are often associated with bond breakage [36–40]. The electronic structure of quantum dots outside graphene is required for the description of the chemisorption bond on graphene.

There are two main lines of research in this work. The first is the computation of the density of states of pure perfect graphene, broadening and quantum shift as a function of energy and normal distance between the adsorbed quantum dot and graphene. The second step consists in the self-consistent calculation of occupation numbers and quasi-energy levels on the adsorbed quantum dot.

THEORETICAL ASSUMPTIONS

There are two different important approaches to the chemisorption process, the first of which involves all calculations of the electronic structure. The second is to create simple models that describe only basic physics, such as the time-independent chemisorption on graphene, depending on the spin of the adsorbed quantum dot, as described by the Anderson–Newns model [41–45].

In our model for a chemisorbed quantum dot on graphene, the following physical characteristics are taken into account: all parameters are related to the adsorbed quantum dot on graphene. The quantum effects of coupling are expressed by the expanding chemisorption function and quantum shift, and then by the electronic structure of the system.

Anderson's model [46] describes a single quantum dot as two energy levels with a local interaction that results in a hybridization with a graphene sheet, allowing resonance tunneling. Coulomb barriers separate the energy level of a localized quantum dot (QD) from graphene. The hybridization function $V(d)$ determines the strength of the interaction. The intra-dot Coulomb energy U separates the spin down level from the spin up level. There Hamiltonian of the system consists of three components:

$$H = H_{\mathrm{QD}} + H_{\mathrm{G}} + H_{\mathrm{hyb}}, \tag{1}$$

$$H_{\mathrm{QD}} = \sum_{\sigma} E_{\mathrm{dot}}^{\sigma} n_{\mathrm{dot}}^{\sigma} + U n_{\mathrm{dot}}^{+\sigma} n_{\mathrm{dot}}^{-\sigma}, \tag{2}$$

$$H_{\mathrm{G}} = \sum_{\mathbf{k}\sigma} E_{\mathbf{k}}^{\sigma} c_{\mathbf{k}}^{\sigma\dagger} c_{\mathbf{k}}^{\sigma}, \tag{3}$$

$$H_{\mathrm{hyb}} = \sum_{\mathbf{k}\sigma} \left(V_{\mathbf{k}}^{\sigma} c_{\mathbf{k}}^{\sigma\dagger} d^{\sigma} + V_{\mathbf{k}}^{\sigma^*} c_{\mathbf{k}}^{\sigma} d^{\sigma\dagger} \right), \tag{4}$$

where the Hamiltonian H_{QD} describes an isolated quantum dot, $E_{\mathrm{dot}}^{\sigma}$ is the energy level of spin up ($+\sigma$)/spin down ($-\sigma$), the second term in eq. (2) accounts for the local Coulomb repulsion U on the dot, $n_{\mathrm{dot}}^{\sigma}$ represents the occupation number of energy levels of the quantum dot: $n_{\mathrm{dot}}^{\sigma} = d^{\sigma\dagger} d^{\sigma}$ and $d^{\sigma\dagger}(d^{\sigma})$ is the creation (annihilation) operator of an electronic state on quantum dot. The Hamiltonian H_{G} describes pure perfect graphene, $c_{\mathbf{k}}^{\sigma\dagger}(c_{\mathbf{k}}^{\sigma})$ is the creation (annihilation) operator of an electronic state with the wave vector $\mathbf{k}$ and energy $E_{\mathbf{k}}^{\sigma}$ on a graphene sheet. H_{hyb} describes the coupling interaction between the adsorbed quantum dot and graphene, $V_{\mathbf{k}}^{\sigma}$ is the hybridization potential, which is given as a function of the normal distance d by the formula:

$$V(d) = V_0 \exp(-\alpha d), \tag{5}$$

where V_0 is the hybridization strength at $d = 0$ and α is the controlled parameter, we assume that the adsorbed quantum dot hybridizes at the top of the carbon atom.

The complexity of the problem is related to the twofold occupancy U of the adsorbent, which for simplicity is often taken as a constant. From the adsorbent perspective, graphene reduces the electrical mobility of the adsorbent. As a result, the confined electrons create their self-energy $\sum(E,d)$, which is proportional to the energy of the system and normal distance [47]:

$$\sum(E,d) = |V(d)|^2 \int \frac{\rho_{\mathrm{G}}(\acute{E})}{(E-\acute{E})^2 + i\lambda^2} d\acute{E}, \quad \lambda \to 0. \tag{6}$$

The real part of self-energy correlates with a quantum shift, which is a change in the energy level:

$$\mathrm{Re}\sum(E,d) = \Lambda(E,d) = |V(d)|^2 \int \frac{(E-\acute{E})\rho_{\mathrm{G}}(\acute{E})}{(E-\acute{E})^2 + \lambda^2} d\acute{E}. \tag{7}$$

The decay rate, i.e., broadening, of an energy level is determined by the imaginary component of the self-energy, which is given by:

$$\mathrm{Im}\sum(E,d) = \Delta(E,d) = -|V(d)|^2 \pi \rho_{\mathrm{G}}(E), \tag{8}$$

while $\rho_{\mathrm{G}}(E)$ is the density of states of pure perfect graphene [48]:

$$\rho_G(E) = \begin{cases} 0 & E < -3t \\ -\dfrac{\rho_0 t}{E} & -3t < E < -t \\ \dfrac{\rho_0}{t}|E| & -t < E < t \\ \dfrac{\rho_0 t}{E} & t < E < 3t \\ 0 & E > 3t \end{cases} \quad \rho_0 = \frac{2}{(1+2\ln 3)t}, \quad (9)$$

where $t = 2.8$ eV [49, 50] is the hopping energy of the nearest carbon atoms of graphene, the width of the valence (π) and conduction (π^*) bands is $3t$, and the energy of the Dirac point $E = 0$ (Fermi level).

Due to the electron–electron interaction ΔE, the energy levels of the quantum dot shift towards each other as it approaches the graphene sheet [51]. The following equation describes the image interaction between electrons in the quantum dot and graphene:

$$\Delta E(d) = \frac{e^2}{4(d + d_0)}, \quad (10)$$

where d_0 denotes the closest approach of the graphene sheet. The energy level of the quantum dot can now be written as:

$$E_{dot}^{\pm\sigma}(E,d) = \varepsilon_{dot} + U n_{dot}^{\mp\sigma}(E,d) + \Delta E(d), \quad (11)$$

where ε_{dot} denotes the quantum energy level of the non-adsorbed quantum dot and $n_{dot}^{\mp\sigma}$ is the occupation number given by [52]:

$$n_{dot}^{\pm\sigma}(E,d) = \int_{-3t}^{3t} \rho_a^{\pm\sigma}(E,d) f(E,T) dE. \quad (12)$$

Here $\rho_a^{\mp\sigma}(E,d)$ is the density of states on the adsorbed quantum dot, and $f(E,T)$ is the Fermi distribution function for the graphene sheet:

$$f(E,T) = \frac{1}{1 + \exp\left(\dfrac{E}{k_B T}\right)}, \quad (13)$$

k_B is the Boltzmann constant; T is the temperature. However, the density of states associated with each quasi-energy level of spin σ ($-\sigma$) is a Lorentz distribution centered at $E_{dot}^{\sigma}\left(E_{dot}^{-\sigma}\right)$ as:

$$= \frac{1}{\pi} \frac{\rho_{dot}^{\sigma}(E,d) \quad \Delta(E,d)}{\left(E - E_{dot}^{\sigma}(E,d) - \Lambda(E,d)\right)^2 + \Delta^2(E,d)}. \quad (14)$$

CALCULATIONS AND DISCUSSION

All equations in the previous section are solved numerically, and it is important to remember that

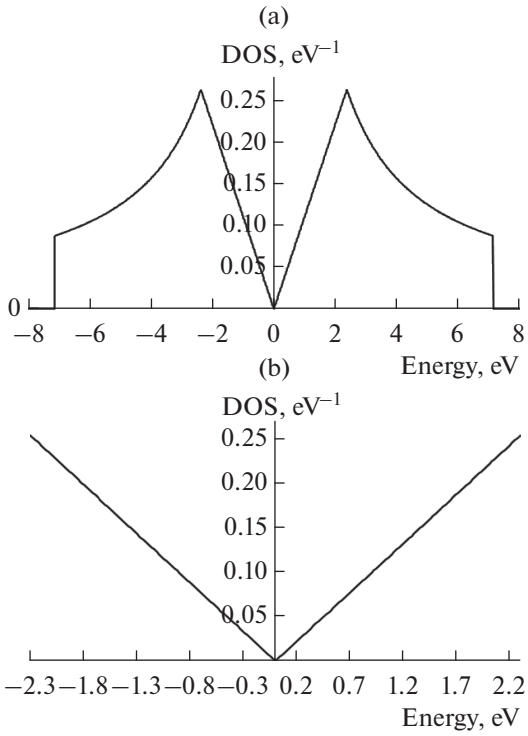

Fig. 1. Density of states (DOS) of pure perfect graphene: (a) over the width of the valence (π) and conduction (π^*) bands; (b) in the strong regime near the Dirac point.

Eqs. (11) and (12) are self-consistently solved. At the initial temperature $T = 300$ K, the Fermi–Dirac statistic is used to fill the electronic level. All functions explaining the chemisorption for any spherical atom-like semiconductor quantum dot on a graphene sheet are included in the self-consistent solution using the Anderson impurity model. The quantum shift and hybridization function are determined as a function of the energy of the system for each d.

Figure 1 shows the density of states $\rho_G(E)$) for a pure perfect graphene sheet. The classical image shift $\Delta E(d)$ in Eq. (10) and the hybridization potential $V(d)$ in Eq. (5) are functions of the distance $d = 20$–0 Å. The values $V_0 = 0.85$ eV and $\alpha = 0.018$ Å^{-1} were substituted into Eq. (5) and various values of d_0 were used in Eq. (10). When the quantum dot approaches the graphene sheet, its energy level shifts due to the polarized charge resulting from the self-inductive field on the graphene sheet.

Notably, when approaching the graphene sheet, the wave functions of electrons in the dot and graphene interfere with each other, which leads to the appearance of transitions through a potential well between the dot and graphene. Thus, the there is a broadening and quantum shift of the dot level. Figure 2 shows the quantum hybridization function (broaden-

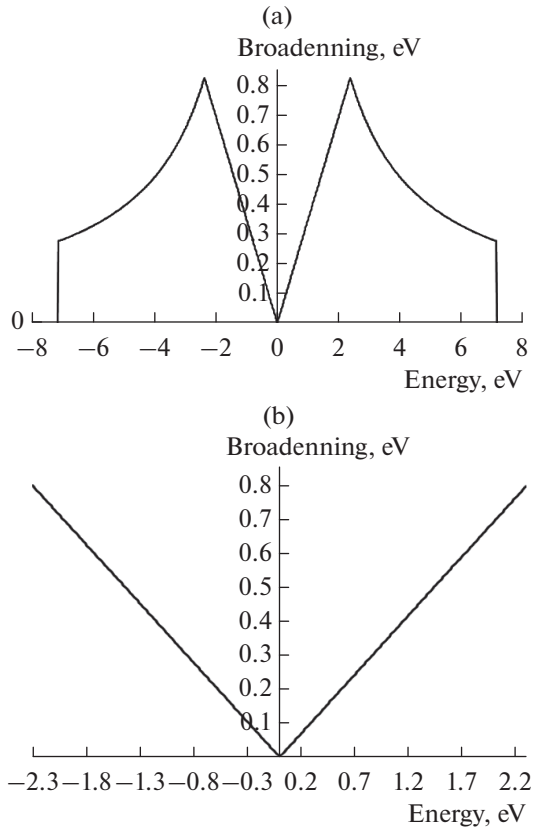

Fig. 2. Hybridization of the energy levels of graphene: (a) over the width of the valence (π) and conduction (π*) bands; (b) in the strong regime near the Dirac point.

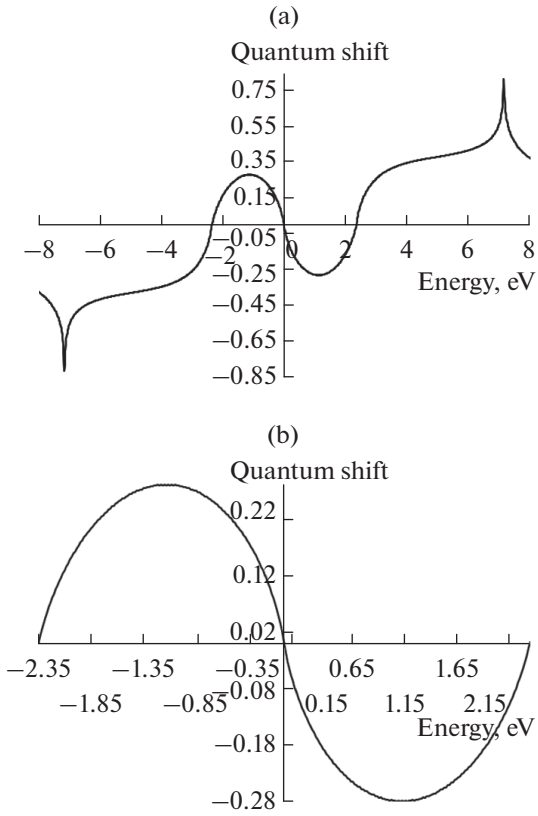

Fig. 3. Quantum shift of the energy levels of graphene: (a) over the width of the valence (π) and conduction (π*) bands; (b) in the strong regime near the Dirac point.

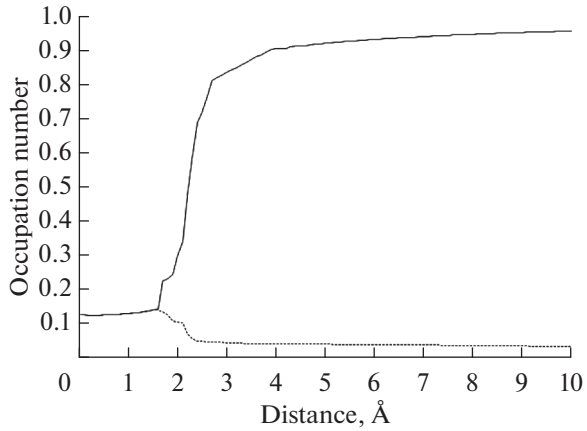

Fig. 4. Distance dependence of the occupation numbers n_{dot}^{σ} (solid line) and $n_{\text{dot}}^{-\sigma}$ (dashed line) of the quasi-energy level of an adsorbed quantum dot.

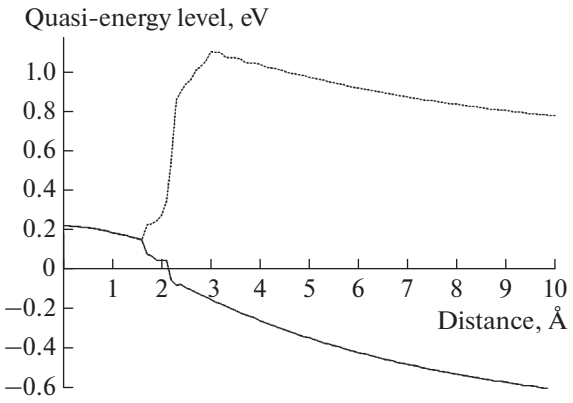

Fig. 5. Distance dependence of the position of the quasi-energy levels E_{dot}^{σ} (solid line) and $E_{\text{dot}}^{-\sigma}$ (dashed line) of an adsorbed quantum dot.

ing $\Delta(E,d)$) and Fig. 3 shows the quantum shift $\Lambda(E,d)$) as a function of energy at $d = d_0$. Attached directly to the carbon atom of the graphene sheet, at the site and at the top of the site, it is placed at $d_0 = 3.5$ Å directly above the graphene sheet.

Solving the problem of Coulomb repulsion in terms of a formula and distance dependence is one of the difficulties that has strained researchers, and is sometimes neglected or generally considered a fixed value in order to accurately describe the charge exchange

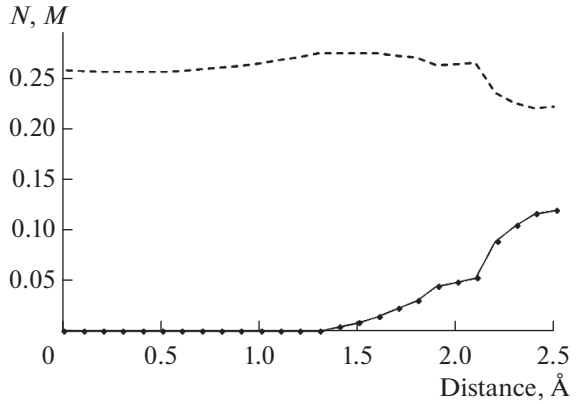

Fig. 6. Distance dependence of the total charge number N (dashed line) and magnetization M (solid line) of the adsorbed quantum dot/graphene.

process between the dot and graphene. Therefore, $\varepsilon_{dot} = 1$ eV, measured with respect to Fermi level and the value of U is chosen to be 1.5 eV.

The variation of the occupation number $n_{dot}^{\mp\sigma}$ as a function of distance is shown in Fig. 4. It shows that the physical solution minimizing the energy of the system is always unique for which n_{dot}^{σ} is greater than $n_{dot}^{-\sigma}$. This is consistent with the results presented in Fig. 5 since E_{dot}^{σ} lies lower than $E_{dot}^{-\sigma}$.

The total number of electrons at the quasi-energy levels of quantum dot $N = n_{dot}^{\sigma} + n_{dot}^{-\sigma}$ (Fig. 6) shows that $0 < N < 1$. To study the magnetic behavior on the adsorption system for a quantum dot/graphene, it is useful to calculate the magnetization $M = n_{dot}^{\sigma} - n_{dot}^{-\sigma}$, as shown in Fig. 6. Since the self-consistent solution is magnetic for all Z values, the magnetization will be dominant for all $d > 1.3$ Å.

The density of states $\rho_a^{\mp\sigma}(E,d)$ on the adsorbed quantum dot at $d = d_0$ as a function of distance and temperature is drawn in Figs. 7 and 8. It includes the broadening of the quasi-level of the adsorbed quantum dot due to the hybridization with the electron sea in graphene. These figures show that $\rho_a^{\sigma}(E,d) = \rho_a^{-\sigma}(E,d)$ are identical or the self-consistent solution is magnetic for $d = d_0$ (i.e., $d = 0$) at both temperatures (500 and 2000 K), but at a distance from graphene (d = 15 Å) they are nonmagnetic; i.e., $\rho_a^{\sigma}(E,d) \neq \rho_a^{-\sigma}(E,d)$. Table 1 highlights these results regardless of the differences between the height of the peaks in the two figures. The influence of temperature on the occupation number and the quasi-energy level of the adsorbed quantum dot is also considered; these

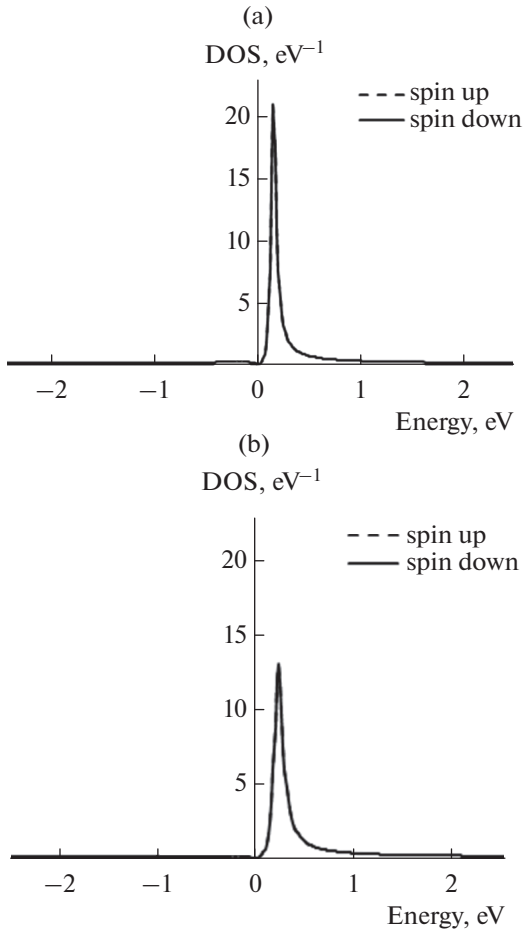

Fig. 7. Localized density of states (DOS) of the adsorbed quantum dot/graphene system ($d = 0$) at: (a) 500; (b) 2000 K.

effects are depicted in Figs. 9 and 10 and summarized in Fig. 11, as well as in Table 2.

The reasons for this similarity are the features of a single quantum dot adsorbed on graphene (in [53] charts of the matching densities of states for several

Table 1. Energy at the peak position estimated from Figs. 7 and 8 explaining the symmetry of the localized density of states at different distances and temperatures

	Energy, eV			
	$d = 0$		$d = 15$ Å	
T, K	n_{dot}^{σ}	$n_{dot}^{-\sigma}$	E_{dot}^{σ}	$E_{dot}^{-\sigma}$
500	0.151	0.151	−0.672	0.672
1000	0.185	0.185	−0.672	0.672
2000	0.235	0.235	−0.638	0.638

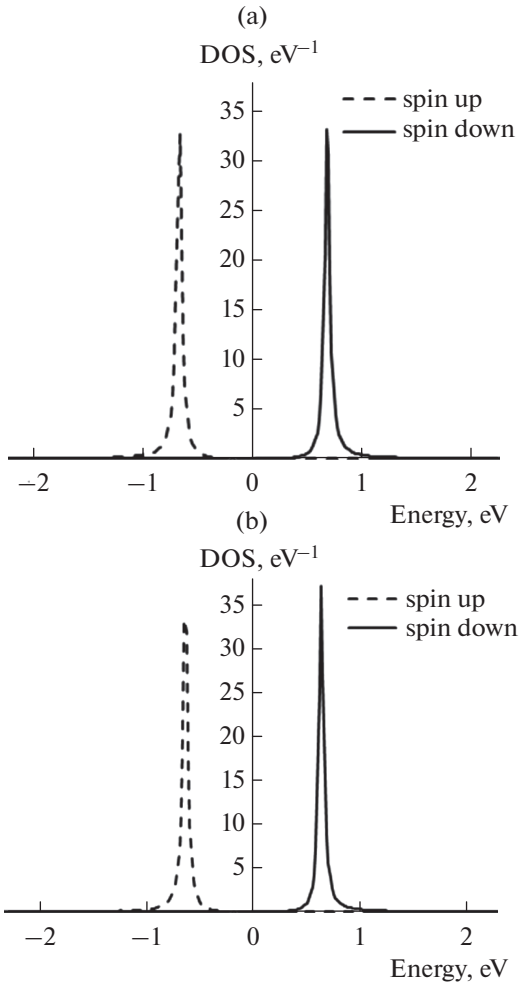

Fig. 8. Localized density of states (DOS) of the quantum dot located at a distance of 15 Å from graphene: at: (a) 500; (b) 2000 K.

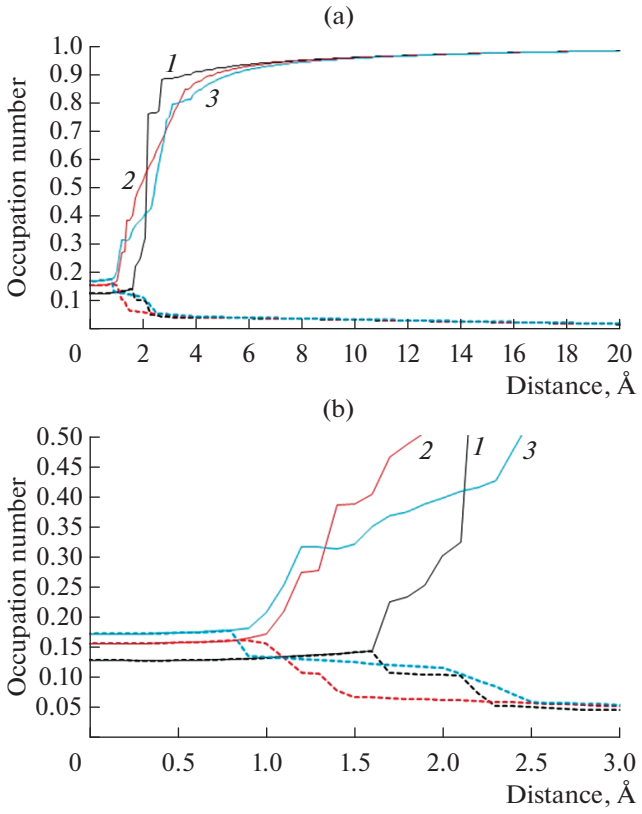

Fig. 9. Spin-dependent occupation numbers as a function of distance for the adsorbed quantum dot/graphene at 300 (line *1*), 750 (line *2*), 1000 K (line *3*): (a) over the entire distance; (b) near the graphene sheet.

examples are given), and the most essential attribute is a pseudogap with the Dirac point in the center. The appearance of the main sharp low-energy maximum for an isolated quantum dot is due to this aspect of the spectrum of single-sheet graphene. The second attribute of the graphene density of states, namely, the existence of maxima at the pseudogap boundaries, also leads to extra side maxima. As a result, all features of density of states of the adsorbed system are explained by the electronic structure of graphene.

Table 2. Spin-independent occupation numbers and quasi-energy levels on a graphene sheet ($d = 0$) and exchange solution distances at various temperatures for an adsorbed quantum dot/graphene

T, K	$E_{dot}^{\mp\sigma}$	$n_{dot}^{\mp\sigma}$	d_{ch}
200	0.218	0.126	1.9
300	0.222	0.129	1.6
500	0.238	0.140	1.1
750	0.263	0.156	0.8
1000	0.287	0.172	0.7
1500	0.328	0.199	1.0
2000	0.361	0.221	1.8
2500	0.388	0.240	2.3

CONCLUSIONS

The adsorption of atom-like spherical semiconductor quantum dots on a perfect pure graphene sheet has been studied using a model Anderson–Newns for chemisorption, or so-called magnetic impurity model, due to the growing interest in studying all cases of graphene (perfect, pure, decorated, etc.) and its use in many applications. In the process of chemisorption on graphene, the quantum dot magnetization (net charge) is not always zero, as follows from magnetism.

It has been found that, due to the weak interaction strength, both the occupation numbers and the quasi-levels are in a nonmagnetic state at distances greater than d_{ch}, while they are in a magnetic state at distances smaller than d_{ch}, i.e., in strong regime. The calculated

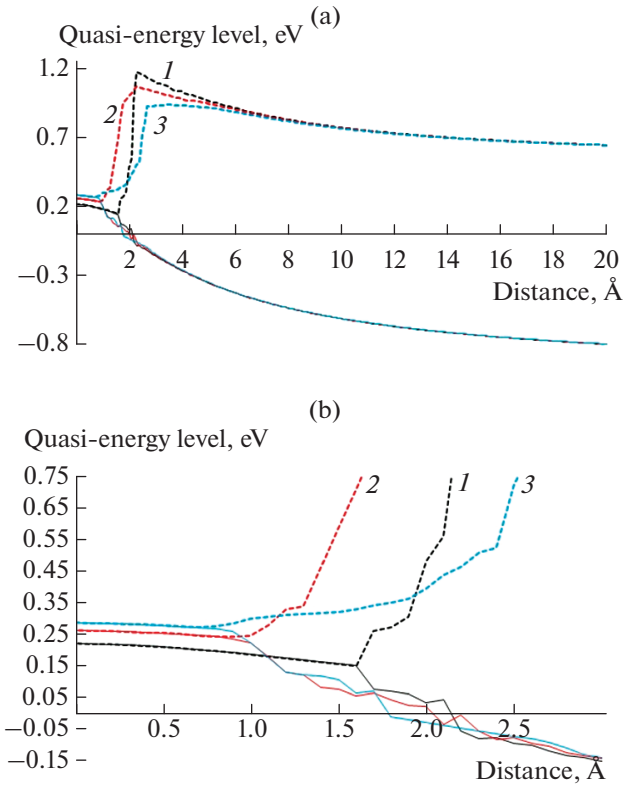

Fig. 10. Spin-dependent quasi-energy level as a function of distance for the adsorbed quantum dot/graphene at 300 (line *1*), 750 (line *2*), 1000 K (line *3*): (a) over the entire distance; (b) near the graphene sheet.

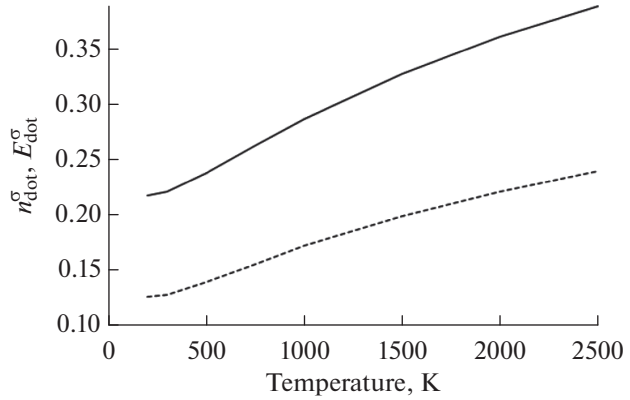

Fig. 11. Temperature dependence of the spin-independent occupation number n^{σ}_{dot} (dashed line) and quasi-energy level E^{σ}_{dot} (solid line) on the graphene sheet for the adsorbed quantum dot/graphene.

values of $n^{\mp\sigma}_{dot}$ are small on the graphene sheet, which indicates the presence of a charge exchange process, while the values of $n^{\mp\sigma}_{dot}$ and their corresponding quasi-energy levels $E^{\mp\sigma}_{dot}$ increase with the increase in temperature as a result of the participation of new energy levels above the Fermi level in occupation numbers, since this is the exchanging point and the transformation of solutions also depends on temperature.

CONFLICT OF INTEREST

The authors declare that they have no conflicts of interest.

REFERENCES

1. C. F. Hirjibehedin, C. P. Lutz, and A. J. Heinrich, Science **312**, 1021 (2006).
2. D. Kitchen, A. Richardella, J.-M. Tang, M. E. Flatté, and A. Yazdani, Nature **442**, 436 (2006).
3. P. Gambardella, S. Rusponi, M. Veronese, S. S. Dhesi, C. Grazioli, A. Dallmeyer, I. Cabria, R. Zeller, P. H. Dederichs, K. Kern, C. Carbone, and H. Brune, Science **300**, 1130 (2003).
4. F. Meier, K. von Bergmann, P. Ferriani, J. Wiebe, M. Bode, K. Hashimoto, S. Heinze, and R. Wiesendander, Phys. Rev. B **74**, 195411 (2006).
5. A. K. Geim and K. S. Novoselov, Nat. Mater. **6**, 183 (2007).
6. V. W. Brar, R. Decker, H. M. Solowan, Y. Wang, L. Maserati, K. T. Chan, H. Lee, C. O. Girit, A. Zettl, S. G. Louie, M. L. Cohen, and M. F. Crommie, Nat. Phys. **7**, 43 (2010).
7. M. Gyamfi, T. Eelbo, M. Wasniowska, and T. O. Wehling, Phys. Rev. B **85**, 161406 (2012).
8. L. Craco, S. S. Carara, T. A. da Silva Pereira, and M. V. Milosevic, Pys. Rev. B **93**, 155417 (2016).
9. S. Yu. Davydov and O. V. Posrednik, Tech. Phys. **62**, 656 (2017).
10. S. Yu. Davydov, Semiconductors **51**, 217 (2017).
11. D. W. Brenner, Phys. Status Solidi B **217**, 23 (2000).
12. A. K. Geim and K. S. Novoselov, Nat. Mater. **6**, 183 (2007).
13. F. Escudero, J. S. Ardenghi, P. Jasen, and A. Juan, Superlattices Microstruct. **113**, 291 (2018).
14. Y. Zhang, J. W. Tan, H. L. Stormer, and P. Kim, Nature **438**, 201 (2005).
15. C. Lee, X. Wei, J. W. Kysar, and J. Hone, Science **321**, 385 (2008).
16. K. I. Bolotin, K. J. Sikes, Z. Jiang, M. Klima, G. Fudenberg, J. Hone, P. Kim, and H. L. Stormer, Solid State Commun. **146**, 351 (2008).
17. S. Chen, L. Brown, M. Levendorf, W. Cai, S.Y. Ju, J. Edgeworth, X. Li, C. W. Magnuson, A. Velamakanni, R. D. Piner, J. Kang, J. Park, and R. S. Ruoff, ACS Nano **5**, 1321(2011).
18. C. L. Lu, C. P. Chang, Y. C. Huang, and R. B. Chen, Phys. Rev. B **73**, 144427 (2006).
19. A. M. Goossens, V. E. Calado, A. Barreiro, K. Watanabe, T. Taniguchi, and L. M. K. Vandersypen, Appl. Phys. Lett. **100**, 073110 (2012).
20. K. S. Novoselov, A. K. Geim, S. V. Morozov, D. Jiang, Y. Zhang, S. V. Dubonos, I. V. Grigorieva, and A. A. Firsov, Science **306**, 666 (2004).
21. S. Yu. Davydov, *Handbook of Graphene*, Ed. by T. Stauber (Scrivener, Manila, 2019), **vol. 2**, pp. 543–586.

22. Y.-W. Tan, Y. Zhang, H. L. Stormer, and P. Kim, Eur. Phys. J. Spectrosc. **148**, 15 (2007).
23. A. H. Castro Neto, F. Guinea, N. M. R. Peres, K. S. Novoselov, and A. K. Geim, Rev. Mod. Phys. **81**, 109 (2009).
24. S. Yu. Davydov, Phys. Solid State **62**, 2459 (2020).
25. M. Titov, Europhys. Lett. **79**, 17004 (2007).
26. A. Schuessler, P. Ostrovsky, I. V. Gornyi, and A. D. Mirlin, Phys. Rev. B **79**, 075405 (2009).
27. J. H. Bardarson, J. Tworzydło, P. W. Brouwer, and C. W. J. Beenakker, Phys. Rev. Lett. **99**, 106801 (2007).
28. T. Stauber, N. M. R. Peres, and F. Guinea, Phys. Rev. B **76**, 205423 (2007).
29. T. O. Wehling, A. V. Balatsky, M. I. Katsnelson, A. I. Lichtenstein, K. Scharnberg, and R. Wiesendanger, Phys. Rev. B **75**, 125425 (2007).
30. F. Schedin, A. K. Geim, S. V. Morozov, E. W. Hill, P. Blake, M. I. Katsnelson, and K. S. Novoselov, Nat. Mater. **6**, 652 (2007).
31. D. C. Elias, R. R. Nair, T. M. G. Mohiuddin, S. V. Morozov, P. Blake, M. P. Halsall, A. C. Ferrari, D. W. Boukhvalov, M. I. Katsnelson, A. K. Geim, and K. S. Novoselov, Science **323**, 610 (2009).
32. X. Song, Q. Chen, M. Dong, G. Yuan, D. Li, B. Ouyang, Y. Wang, and W. Sun, Chem. Phys. Lett. **738**, 136896 (2020).
33. P. M. Ostrovsky, I. V. Gornyi, and A. D. Mirlin, Phys. Rev. B **74**, 235443 (2006).
34. P. M. Ostrovsky, M. Titov, S. Bera, I. V. Gornyi, and A. D. Mirlin, arXiv:1006.3299 (2010).
35. S. Herschfield, J. H. Davies, and J. W. Wilkins, Phys. Rev. Lett. **67**, 3720 (1991).
36. N. S. Wingreen and Y. Meir, Phys. Rev. B **49**, 11040 (1994).
37. H. K. Fadel, Z. Z. Alisultanov, N. A. Mirzegasanova, and G. M. Musaev, J. Surf. Invest: X-ray, Synchrotron Neutron Tech. **8**, 675 (2014).
38. Z. Z. Alisultanov, N. A. Mirzegasanova, G. M. Musaev, and H. K. Fadel, Eng. Phys. **11**, 21 (2013).
39. H. K. Al-Edany, J. Basrah Res. (Sci.) **31**, 19 (2005).
40. P. W. Anderson, Phys. Rev. **124**, 41 (1961).
41. H. K. Al-Edany and J. M. Al-Much, J. Basrah Res. (Sci.) **28**, 136 (2002).
42. H. K. Al-Edany and J. M. Al-Much, J. Basrah Res. (Sci.) **29**, 85 (2003).
43. H. K. Al-Edany and M. M. Al-Samer, J. Basrah Res. (Sci.) **31**, 23 (2005).
44. H. K. Al-Edany, J. Basrah Res. (Sci.) **34**, 9 (2008).
45. D. M. Newns, Phys. Rev. **178**, 1123 (1969).
46. A. H. Castro Neto, V. N. Kotov, J. Nilsson, V. M. Pereira, N. M. R. Peres, and B. Uchoa, arXiv: 0812.2072 (2008).
47. T. O. Wehling, M. I. Katsnelson, and A. I. Lichtenstein, Chem. Phys. Lett. **476**, 125 (2009).
48. S. Yu. Davydov, World Appl. Sci. J. **27**, 1574 (2013).
49. L. Hao, H.-Yan Lu, and C. S. Ting, Phys. Rev. Mater. **3**, 024003 (2019).
50. T. O. Wehling, E. Sasioglu, C. Friedrich, A. I. Lichtenstein, M. I. Katsnelson, and S. Blügel, Phys. Rev. Lett. **106**, 236805 (2011).
51. B. Kjollerstrom, D. J. Scalapino, and J. R. Schrieffer, Phys. Rev. **148**, 665 (1966).
52. H. K. Fadel, A. K. Nokhov, and G. M. Mysaev, Herald Dagestan State Univ. **6**, 54 (2012).
53. S. Yu. Davydov and G. I. Sabirova, Phys. Solid State **53**, 654 (2011).